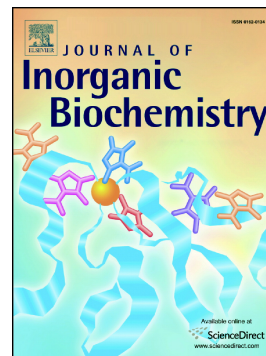


Accepted Manuscript

New (arene)ruthenium(II) complexes of 4'aryl'4H'naphthopyrans with anticancer and anti-vascular activities

Florian Schmitt, Jana Kasparikova, Viktor Brabec, Gerrit Begemann, Rainer Schobert, Bernhard Biersack



PII: S0162-0134(17)30634-7
DOI: doi:[10.1016/j.jinorgbio.2018.03.013](https://doi.org/10.1016/j.jinorgbio.2018.03.013)
Reference: JIB 10464

To appear in: *Journal of Inorganic Biochemistry*

Received date: 11 September 2017
Revised date: 6 March 2018
Accepted date: 22 March 2018

Please cite this article as: Florian Schmitt, Jana Kasparikova, Viktor Brabec, Gerrit Begemann, Rainer Schobert, Bernhard Biersack , New (arene)ruthenium(II) complexes of 4'aryl'4H'naphthopyrans with anticancer and anti-vascular activities. The address for the corresponding author was captured as affiliation for all authors. Please check if appropriate. Jib(2017), doi:[10.1016/j.jinorgbio.2018.03.013](https://doi.org/10.1016/j.jinorgbio.2018.03.013)

This is a PDF file of an unedited manuscript that has been accepted for publication. As a service to our customers we are providing this early version of the manuscript. The manuscript will undergo copyediting, typesetting, and review of the resulting proof before it is published in its final form. Please note that during the production process errors may be discovered which could affect the content, and all legal disclaimers that apply to the journal pertain.

JINORGBIO_2017_482_R3

**New (arene)ruthenium(II) complexes of 4-aryl-4*H*-naphthopyrans with
anticancer and anti-vascular activities**

Florian Schmitt^a, Jana Kasparikova^b, Viktor Brabec^c, Gerrit Begemann^d, Rainer Schobert^{a,*}
and Bernhard Biersack^a

^a Department of Chemistry, University of Bayreuth, Universitaetsstrasse 30, 95440 Bayreuth, Germany

^b Department of Biophysics, Faculty of Science, Palacky University, 17. Listopadu 12, CZ-77146 Olomouc,
Czech Republic

^c Institute of Biophysics, Academy of Sciences of the Czech Republic, CZ-61265 Brno, Czech Republic

^d Developmental Biology, University of Bayreuth, Universitaetsstrasse 30, 95440 Bayreuth, Germany.

* Corresponding author. E-mail address: Rainer.Schobert@uni-bayreuth.de, Fax: 0049 (0)921 552671

Abstract

A series of four 2-amino-3-cyano-4-(3/4-pyridyl)-4*H*-benzo[h]chromenes **2a-d** and their dichlorido(*p*-cymene)ruthenium(II) complexes **3a-d** were tested for antiproliferative, vascular-disruptive, anti-angiogenic and DNA-binding activity. The coordination of the 4-pyridyl-4*H*-naphthopyrans **2** to ruthenium led to complexes with pleiotropic effects. Unlike the free ligands **2a-d**, their ruthenium complexes **3a-d** showed a significant affinity for DNA as demonstrated by electrophoretic mobility shift assays (EMSA) and ethidium bromide assays. Binding of **3a-d** to calf thymus DNA proceeded about 10-times faster compared with cisplatin. Treatment of HT-29 colon carcinoma, 518A2 melanoma and MCF-7^{Topo} breast cancer cells with **3a** and **3b** caused an accumulation of cells in the G2/M phase and an increase of the fraction of mitotic cells in the case of HT-29, due to alterations of the microtubule cytoskeleton as shown by immunofluorescence staining. Complexes **3b-c** showed a dual effect on the vascular system. They suppressed angiogenesis in zebrafish embryos and they destroyed the vasculature of the chorioallantoic membrane (CAM) in fertilized chicken eggs. They also inhibited the vasculogenic mimicry, typical of U-87 glioblastoma cells in tube formation assays.

Keywords: Vascular-disrupting agents (VDA); naphthopyran; (arene)ruthenium(II) complexes; DNA binding; zebrafish.

1. Introduction

Cis-diamminedichloroplatinum(II) (cisplatin, CDDP) has represented the gold standard of metal-based chemotherapeutics since the serendipitous discovery of its anticancer effect in the 1960s [1]. Even though the treatment of various solid tumors with cisplatin is quite successful, this comes at the price of severe side effects such as neural damage and cardio- as well as nephrotoxicity which limit its clinical applicability [2,3]. Many common types of cancer do not respond to cisplatin treatment, and acquired drug resistance is quite frequently observed. Hence, there is a need for new metal-based chemotherapeutics which overcome these limitations. Against the backdrop of metastatic tumors claiming far more lives than the

primary tumor, anti-metastatic ruthenium complexes such as NAMI-A (imidazolium *trans*-imidazole-tetrachlororuthenate) [4] or KP1019 (trans-[tetrachlorobis(1H-indazole)ruthenate(III)]) [5], which already passed clinical trials, have attracted great attention. Although their detailed mechanism of action is still not fully understood, these Ru(III) complexes are thought to get activated intracellularly by reduction to distinctly more cytotoxic Ru(II) species [6]. In addition, the transport and the selective cellular uptake of Ru(III) complexes via transferrin and the transferrin receptors appears to play a decisive role [7,8]. Antitumoral (arene)ruthenium(II) complexes constitute another important class. The arene ligand of these so-called “piano stool” complexes is believed to stabilize the bioactive Ru(II) state [9]. They are particularly attractive to the medicinal chemist because of their ease of synthesis and their structural variability. (Arene)ruthenium(II) complexes may feature various anticancer properties. While some derivatives display an anti-metastatic mode of action similar to NAMI-A, involving their binding to proteins, others bind to DNA in a way comparable with the DNA interaction of cisplatin [9-13]. The introduction of ligands with appropriate intrinsic anticancer activities may give rise to pleiotropic complexes with synergistic or additive effects [14]. We have recently observed that the complexation of highly toxic ligands attenuates their general toxicity leading to more tumor-selective Ru(II) complexes [15]. Herein, we report on a series of new (arene)ruthenium(II) complexes bearing naphthopyran ligands. Naphthopyrans such as LY290181 [2-amino-4-(3-nitrophenyl)-4H-naphtho(1,2-b)pyran-3-carbonitrile] are microtubule destabilizing agents (MDA) which exert their effect by binding to tubulin, causing the inhibition of the tubulin polymerization which leads to alterations of the microtubule cytoskeleton [16-19]. Because of these alterations, the spindle apparatus cannot be formed correctly causing the arrest of the cell cycle in G2/M phase and the induction of apoptosis [19]. Hence, these MDA are highly anti-proliferative [16-18,20-22]. Moreover, the destruction of the microtubule cytoskeleton leads to a reduction of the mechanical stability of cells and of the irregular tumor blood vessels, which eventually

causes their collapse and induces tumor cell necrosis [16,17,22]. By the synthesis of (arene)ruthenium(II) complexes bearing naphthopyran ligands we investigated if ruthenation leads to complexes featuring a combination of typical naphthopyran properties such as antiproliferative [17,18,20-22], vascular-disruptive [17,22] and microtubule destabilizing activity [17-19], and of typical (arene)ruthenium(II) properties such as DNA binding [8,9,23,24] and anti-angiogenic activity [2,13].

((Figure 1 near here))

2. Experimental

2.1. General

Melting points were determined with a Gallenkamp apparatus and are uncorrected. IR spectra were recorded on a Perkin–Elmer One FT-IR spectrophotometer. Magnetic resonance (NMR) spectra were recorded under conditions as indicated on a Bruker Avance 300 spectrometer. Chemical shifts (δ) are given in parts per million downfield from TMS as internal standard. Mass spectra were recorded using a Varian MAT 311A (EI) or a UPLC/Orbitrap MS system (ESI). Elemental analyses were carried out with a Perkin–Elmer 2400 CHN elemental analyzer. Satisfactory microanalyses (C, ± 0.2 ; H, ± 0.1) were obtained for all new complexes.

2.2. Chemistry

All starting compounds were purchased from Sigma-Aldrich. Compounds **2a**, **2b**, and RuPy were prepared according to literature procedures [25-27].

2-Amino-6-chloro-4-(pyridin-3-yl)-4H-benzo[h]chromene-3-carbonitrile 2c

Pyridine-3-carboxaldehyde (107 mg, 1.0 mmol) and malononitrile (70 mg, 1.0 mmol) were dissolved in MeCN (5 mL) and three drops of Et₃N were added. The reaction mixture was stirred at room temperature for 30 min. 4-Chloro-1-naphthol (178 mg, 1.0 mmol) was added and the reaction mixture was stirred at room temperature for 1 h. The formed precipitate was

collected, washed with MeCN and *n*-hexane and dried in vacuum. Yield: 196 mg (0.59 mmol, 59%); colorless solid of m.p. 255 °C; $\nu_{\max}(\text{ATR})/\text{cm}^{-1}$ 3441, 3037, 2187, 1651, 1629, 1609, 1579, 1569, 1481, 1428, 1405, 1372, 1289, 1277, 1260, 1203, 1172, 1155, 1112, 1058, 1043, 1030, 963, 942, 873, 862, 829, 762, 744, 716, 682; $^1\text{H NMR}$ (300 MHz, DMSO- d_6) δ 5.03 (1 H, s), 7.3-7.4 (4 H, m), 7.6-7.7 (1 H, m), 7.7-7.8 (2 H, m), 8.1-8.2 (1 H, m), 8.3-8.4 (1 H, m), 8.4-8.5 (1 H, m), 8.6 (1 H, s); $^{13}\text{C NMR}$ (75.5 MHz, DMSO- d_6) δ 38.5, 55.6, 118.2, 120.6, 122.1, 124.4, 124.5, 124.8, 126.3, 128.4, 129.1, 129.9, 136.1, 141.0, 141.1, 142.8, 149.1, 149.2, 149.3, 160.6; m/z (EI) 335 (12) [M^+], 333 (35) [M^+], 257 (55), 255 (100), 193 (15). Anal. calcd. for $\text{C}_{19}\text{H}_{12}\text{ClN}_3\text{O}$: C, 68.37; H, 3.62. Found: C, 68.13; H, 3.55.

2-Amino-6-chloro-4-(pyridin-4-yl)-4H-benzo[h]chromene-3-carbonitrile 2d

Pyridine-4-carboxaldehyde (107 mg, 1.0 mmol) and malononitrile (70 mg, 1.0 mmol) were dissolved in MeCN (5 mL) and three drops of Et_3N were added. The reaction mixture was stirred at room temperature for 30 min. 4-Chloro-1-naphthol (178 mg, 1.0 mmol) was added and the reaction mixture was stirred at room temperature for 1 h. The formed precipitate was collected, washed with MeCN and *n*-hexane and dried in vacuum. Yield: 200 mg (0.60 mmol, 60%); colorless solid of m.p. 246 °C; $\nu_{\max}(\text{ATR})/\text{cm}^{-1}$ 3333, 3292, 3054, 2867, 2198, 1664, 1614, 1596, 1571, 1404, 1372, 1281, 1260, 1202, 1173, 1114, 1067, 1053, 1027, 1001, 963, 942, 875, 860, 817, 766, 747, 679; $^1\text{H NMR}$ (300 MHz, DMSO- d_6) δ 4.99 (1 H, s), 7.30 (2 H, dd, $J = 6.1$ Hz, 1.6 Hz), 7.34 (1 H, s), 7.39 (2 H, s), 7.7-7.8 (2 H, m), 8.1-8.2 (1 H, m), 8.3-8.4 (1 H, m), 8.53 (2 H, dd, $J = 6.1$ Hz, 1.6 Hz); $^{13}\text{C NMR}$ (75.5 MHz, DMSO- d_6) δ 39.9, 54.7, 117.1, 119.9, 121.5, 122.8, 123.9, 125.6, 125.9, 127.9, 128.6, 129.5, 142.4, 150.2, 153.2, 160.3; m/z (EI) 335 (11) [M^+], 333 (33) [M^+], 257 (53), 255 (100), 193 (16). Anal. calcd. for $\text{C}_{19}\text{H}_{12}\text{ClN}_3\text{O}$: C, 68.37; H, 3.62. Found: C, 68.16; H, 3.54.

Dichlorido(p-cymene)[2-amino-4-(pyridin-3-yl)-4H-benzo[h]chromene-3-carbonitrile]ruthenium(II)

3a

2a (68 mg, 0.23 mmol) was dissolved in CH_2Cl_2 (5 mL) and five drops of MeOH. $[\text{Ru}(p\text{-cymene})\text{Cl}_2]_2$ (70 mg, 0.12 mmol) was added and the reaction mixture was vigorously stirred for 30 min. Ethyl acetate / *n*-hexane (1:4, 50 mL) was added and the formed precipitate was collected,

washed with *n*-hexane and dried in vacuum. Yield: 110 mg (0.18 mmol, 79%); amber solid of m.p. 173-175 °C; $\nu_{\max}(\text{ATR})/\text{cm}^{-1}$ 3302, 3153, 3057, 2964, 2186, 1652, 1629, 1598, 1505, 1472, 1409, 1375, 1290, 1263, 1188, 1104, 1057, 1023, 874, 815, 753, 732, 702; $^1\text{H NMR}$ (300 MHz, CDCl_3) δ 1.28 (6 H, d, $J = 6.9$ Hz), 2.09 (3 H, s), 2.9-3.0 (1 H, m), 4.95 (2 H, s), 4.98 (1 H, s), 5.2-5.3 (2 H, m), 5.43 (1 H, d, $J = 5.9$ Hz), 5.49 (1 H, d, $J = 5.9$ Hz), 6.88 (1 H, d, $J = 8.6$ Hz), 7.1-7.2 (1 H, m), 7.3-7.4 (1 H, m), 7.5-7.6 (3 H, m), 7.7-7.8 (1 H, m), 8.15 (1 H, d, $J = 8.1$ Hz), 8.9-9.0 (1 H, m), 9.08 (1 H, s); $^{13}\text{C NMR}$ (75.5 MHz, CDCl_3) δ 18.1, 22.1, 22.5, 30.7, 38.7, 59.7, 82.4, 83.3, 97.3, 103.7, 114.4, 119.6, 120.7, 123.0, 124.8, 125.5, 125.8, 127.0, 127.3, 127.9, 133.7, 137.5, 141.0, 143.7, 153.7, 154.3, 159.2; m/z (EI) 299 (17), 234 (3), 232 (4), 221 (100), 119 (39); m/z (ESI) 563.8 (13), 390.3 (13), 301.3 (80), 282.4 (100), 221.2 (70). Anal. calcd. for $\text{C}_{29}\text{H}_{27}\text{Cl}_2\text{N}_3\text{ORu}$: C, 57.52; H, 4.49. Found: C, 57.40; H, 4.43.

Dichlorido(p-cymene)[2-amino-4-(pyridin-4-yl)-4H-benzo[h]chromene-3-carbonitrile]ruthenium(II)

3b

2b (68 mg, 0.23 mmol) and $[\text{Ru}(p\text{-cymene})\text{Cl}_2]_2$ (70 mg, 0.12 mmol) were dissolved in CH_2Cl_2 (5 mL) and the reaction mixture was vigorously stirred for 30 min. Ethyl acetate / *n*-hexane (1:4, 50 mL) was added and the formed precipitate was collected, washed with *n*-hexane and dried in vacuum. Yield: 110 mg (0.18 mmol, 79%); amber solid of m.p. 218-219 °C; $\nu_{\max}(\text{ATR})/\text{cm}^{-1}$ 3273, 3159, 3051, 2961, 2185, 1652, 1630, 1608, 1574, 1495, 1471, 1403, 1375, 1290, 1264, 1189, 1103, 1062, 1023, 963, 860, 804, 771, 756, 734, 690, 669, 649, 618; $^1\text{H NMR}$ (300 MHz, $\text{CDCl}_3/\text{DMF-d}_7$) δ 1.07 (6 H, d, $J = 7.0$ Hz), 1.87 (3 H, s), 2.7-2.8 (1 H, m), 4.70 (1 H, s), 5.02 (2 H, d, $J = 6.2$ Hz), 5.2-5.3 (2 H, m), 6.02 (2 H, s), 6.70 (1 H, d, $J = 8.6$ Hz), 6.98 (2 H, d, $J = 6.6$ Hz), 7.3-7.4 (3 H, m), 7.5-7.6 (1 H, m), 7.9-8.0 (1 H, m), 8.69 (2 H, d, $J = 6.6$ Hz); $^{13}\text{C NMR}$ (125 MHz, $\text{CDCl}_3/\text{DMF-d}_7$) δ 17.6, 21.7, 30.1, 40.4, 53.1, 81.9, 96.4, 103.1, 114.3, 119.3, 120.5, 122.8, 123.3, 124.0, 125.0, 126.3, 126.6, 127.2, 133.1, 143.3, 154.5, 154.9, 160.2; m/z (ESI) 563.8 (9), 300.3 (28), 282.4 (100), 221 (31), 100.2 (29). Anal. calcd. for $\text{C}_{29}\text{H}_{27}\text{Cl}_2\text{N}_3\text{ORu}$: C, 57.52; H, 4.49. Found: C, 57.43; H, 4.45.

Dichlorido(p-cymene)[2-amino-6-chloro-4-(pyridin-3-yl)-4H-benzo[h]chromene-3-carbonitrile]ruthenium(II) 3c

2c (76 mg, 0.23 mmol) was dissolved in CH_2Cl_2 (5 mL) and five drops of MeOH. $[\text{Ru}(p\text{-cymene})\text{Cl}_2]_2$

(70 mg, 0.12 mmol) was added and the reaction mixture was vigorously stirred for 30 min. Ethyl acetate / *n*-hexane (1:4, 50 mL) was added and the formed precipitate was collected, washed with *n*-hexane and dried in vacuum. Yield: 120 mg (0.19 mmol, 84%); amber solid of m.p. 195-197 °C; $\nu_{\max}(\text{ATR})/\text{cm}^{-1}$ 3290, 3150, 3057, 2964, 2191, 1651, 1626, 1594, 1567, 1471, 1431, 1405, 1368, 1286, 1261, 1204, 1174, 1111, 1058, 1027, 964, 940, 863, 838, 804, 764, 744, 705; $^1\text{H NMR}$ (300 MHz, CDCl_3) δ 1.27 (6 H, d, $J = 6.9$ Hz), 2.07 (3 H, s), 2.9-3.0 (1 H, m), 4.91 (1 H, s), 5.08 (1 H, s), 5.2-5.3 (2 H, m), 5.42 (1 H, d, $J = 5.9$ Hz), 5.47 (1 H, d, $J = 5.9$ Hz), 6.99 (1 H, s), 7.2-7.3 (1 H, m), 7.3-7.4 (1 H, m), 7.6-7.7 (2 H, m), 8.1-8.2 (2 H, m), 8.9-9.0 (1 H, m), 9.06 (1 H, s); $^{13}\text{C NMR}$ (75.5 MHz, CDCl_3) δ 18.1, 22.1, 22.4, 30.7, 38.6, 59.5, 82.4, 83.2, 97.3, 103.8, 114.8, 119.3, 121.4, 124.1, 124.8, 125.2, 127.9, 128.3, 128.7, 130.8, 137.4, 140.4, 142.8, 153.9, 154.4, 159.0; m/z (EI) 335 (6), 333 (20), 257 (34), 255 (100), 193 (12), 134 (17), 119 (55), 91 (12), 36 (15); m/z (ESI) 563.8 (14), 336.3 (83), 282.4 (100), 255.1 (26). Anal. calcd. for $\text{C}_{29}\text{H}_{26}\text{Cl}_3\text{N}_3\text{ORu}$: C, 54.43; H, 4.09. Found: C, 54.31; H, 4.02.

Dichlorido(p-cymene)[2-amino-6-chloro-4-(pyridin-4-yl)-4H-benzo[h]chromene-3-carbonitrile]ruthenium(II) 3d

2d (76 mg, 0.23 mmol) and $[\text{Ru}(p\text{-cymene})\text{Cl}_2]_2$ (70 mg, 0.12 mmol) were dissolved in CH_2Cl_2 (5 mL) and the reaction mixture was vigorously stirred for 30 min. Ethyl acetate / *n*-hexane (1:4, 50 mL) was added and the formed precipitate was collected, washed with *n*-hexane and dried in vacuum. Yield: 104 mg (0.16 mmol, 71%); amber solid of m.p. >220 °C; $\nu_{\max}(\text{ATR})/\text{cm}^{-1}$ 3282, 3160, 3066, 2964, 2186, 1648, 1627, 1608, 1594, 1570, 1499, 1473, 1406, 1369, 1281, 1261, 1206, 1174, 1113, 1062, 1024, 963, 939, 867, 839, 805, 767, 732, 681, 646, 618; $^1\text{H NMR}$ (300 MHz, $\text{CDCl}_3/\text{DMF-d}_7$) δ 1.06 (6 H, d, $J = 7.0$ Hz), 1.88 (3 H, s), 2.7-2.8 (1 H, m), 4.68 (1 H, s), 5.03 (2 H, d, $J = 6.3$ Hz), 5.2-5.3 (2 H, m), 6.14 (2 H, s), 6.84 (1 H, s), 6.99 (2 H, d, $J = 6.6$ Hz), 7.4-7.5 (2 H, m), 7.9-8.0 (1 H, m), 8.0-8.1 (1 H, m), 8.71 (2 H, d, $J = 6.6$ Hz); $^{13}\text{C NMR}$ (75 MHz, $\text{CDCl}_3/\text{DMF-d}_7$) δ 17.6, 21.7, 30.2, 40.3, 53.1, 81.9, 82.0, 96.5, 103.2, 114.8, 121.1, 123.3, 123.9, 124.1, 127.2, 127.5, 127.8, 130.2, 142.4, 154.4, 154.7, 160.0; m/z (ESI) 563.8 (10), 334.2 (53), 282.4 (100), 255.1 (33), 97.2 (24). Anal. calcd. for $\text{C}_{29}\text{H}_{26}\text{Cl}_3\text{N}_3\text{ORu}$: C, 54.43; H, 4.09. Found: C, 54.29; H, 4.04.

2.3. Biological evaluation

2.3.1. Cell culture

MCF-7^{Topo} (ACC-115) breast carcinoma, KB-V1^{Vbl} (ACC-149) cervix carcinoma, HT-29 (ACC-299), DLD-1 (ACC-278) and HCT-116 (ACC-581) colon carcinoma, 518A2 (Department of Radiotherapy, Medical University of Vienna, Austria) melanoma, Panc-1 (ACC-783) pancreatic ductular adenocarcinoma, and U-87 (ATCC: HTB-14) glioblastoma cells were cultivated in Dulbecco's Modified Eagle Medium (DMEM; supplemented with 10% fetal bovine serum (FBS) and 1% Antibiotic-Antimycotic) at 37 °C, 5% CO₂ and 95% humidity. Human dermal fibroblasts HDFa (ATCC: PCS-201-012TM) were grown in DMEM supplemented with 10% FBS, 1% Antibiotic-Antimycotic, and 2 mM glutamine at 37 °C, 5% CO₂, and 95% humidity. The maximum-tolerated dose of topotecan or vinblastine was added to the cell culture medium 24 h after every cell passage to keep the MCF-7^{Topo} or the KB-V1^{Vbl} cells resistant. Only mycoplasma-free cultures were used.

2.3.2. MTT assay

All cell lines were seeded at a concentration of 5×10^4 cells/mL in 96-well plates (100 μ L/well), except for U-87 glioblastoma cells, and HDFa human dermal fibroblasts, which were seeded at a concentration of 1×10^5 cells/mL. After 24 h of incubation, the cells were treated with various concentrations (100 μ M - 0.5 nM) of the test compounds, cisplatin, RuPy, or vehicle (DMF; maximum concentration 1%) for 24 or 72 h at 37 °C. Then, 12.5 μ L of a 0.5% MTT [3-(4,5-dimethylthiazol-2-yl)-2,5-diphenyltetrazolium bromide] solution were added per well and incubated for 2 h at 37 °C to convert water-soluble MTT into insoluble formazan crystals. After centrifugation (300 g, 5 min, 4 °C) the medium was discarded and the formazan was dissolved in 25 μ L of DMSO containing 10% SDS and 0.6% acetic acid for at least 2 h at 37 °C. Then, the absorbance at wavelength 570 nm (formazan) and 630 nm (background) was measured with a microplate reader (Tecan). Each experiment was carried out in quadruplicate and the IC₅₀ values determined as means \pm SD (standard deviation) with respect to control cells set to 100% viable cells.

2.3.3. Electrophoretic mobility shift assay (EMSA) with pBR322 plasmid DNA

The electrophoretic mobility shift assay (EMSA) was used to study the compound-induced unwrapping of covalently closed circular (*ccc*) topofom of pBR322 plasmid DNA (Thermo Scientific). The circular plasmid DNA (75 μ g/mL) in TE buffer (10 mM Tris-HCl, 1 mM EDTA, pH

8.5) was incubated with varying concentrations of the test compounds or positive control (cisplatin) at 37 °C for 24 h. Then, samples were subjected to gel electrophoresis using 1% agarose gels in 0.5× TBE buffer (89 mM Tris, 89 mM boric acid, 25 mM EDTA, pH 8.3). After staining the gels with ethidium bromide (10 µg/mL), pictures of the gels were taken under UV excitation.

2.3.4. Ethidium bromide saturation assay

The extent of the compounds' DNA interactions was additionally assessed by a fluorescence-based ethidium bromide staining assay [28]. 100 µL of a 10 µg/mL solution of salmon sperm DNA in 1× TE buffer (Sigma-Aldrich) was pipetted in a black 96-well plate and incubated with concentrations of the compounds or cisplatin in the standard range (0, 25, 50, 75 and 100 µM) for 2 h at 37 °C.[29] Then, 100 µL ethidium bromide in 1× TE buffer was added to reach a final concentration of 5 µg/mL. After 5 min of incubation, the fluorescence ($\lambda_{\text{ex}} = 535 \text{ nm}$, $\lambda_{\text{em}} = 595 \text{ nm}$) was monitored for each well using a microplate reader (Tecan). Each fluorescence value was corrected by ethidium bromide background (samples without DNA) and the compounds' possible intrinsic fluorescence. The resulting values were expressed as percent of vehicle (100% ethidium bromide binding = 100% fluorescence). Reduced fluorescence is representative for impaired ethidium bromide-DNA adducts due to intercalation sites being blocked by the test compounds. All experiments were carried out in triplicates resulting in the mean \pm SD of relative ethidium bromide fluorescence.

2.3.5. DNA binding in cell free media

Solutions of double-helical calf thymus DNA (42% G + C) at a concentration of 64 µg mL⁻¹ were incubated with **3a-d** in NaClO₄ (10 mM) at 37 °C so that the molar ratio of ruthenium complex to nucleotide residues was 0.04. Aliquots of the reaction mixtures were withdrawn at various time intervals, the reaction was stopped by addition of NaCl (1 M), and samples were quickly cooled in a dry ice bath. The samples were exhaustively dialyzed first against 1 M NaCl and subsequently against water to remove free unbound ruthenium complexes. The concentrations of DNA and the content of ruthenium associated with DNA were determined by absorption spectrophotometry and FAAS (Varian AA240Z), respectively.

2.3.6. Chorioallantoic membrane (CAM) assay in fertilized chicken eggs [30]

Fertilized white leg horn chicken eggs (VALO Biomedica) were incubated at 37 °C and 50-60% humidity until day six past fertilization. Then, the eggs were opened by cutting a window of 2- 3 cm diameter in the eggshell at the more rounded pole and incubated for a further 24 h. After placing a thin silicon ring ($\varnothing = 5$ mm) onto the chorioallantoic membrane with its developing blood vessel system, the customarily used amount of test compounds (10 μ L of a 0.5 mM solution) was pipetted inside these rings. The effect on the vasculature was documented 0, 6 and 24 h past application (hpa) with a light microscope (Traveller, 60 \times magnification).

2.3.7. Tube formation assay

U-87 glioblastoma cells (2.5×10^6 cells/mL, 100 μ L/well) were seeded in 96-well plates on thin layers of matrigel (Corning) and subsequently treated with **3b** (500 nM), **3c** (1 μ M) or vehicle (DMF) for 24 h. The test compounds' effect on the tube formation was documented with a microscope (Zeiss, 100 \times magnification). The viability of the cells was determined by MTT assay.

2.3.8. Fluorescence labeling of microtubules

518A2 melanoma cells (1×10^5 cells/mL; 500 μ L/well) were grown for 24 h on glass coverslips at 37 °C. Then, the cells were exposed to **3a-d** (500 nM), or vehicle (DMF) for 3 h. After fixation of the cells in 3.7% formaldehyde in PBS for 20 min at room temperature, the cells were blocked and permeabilized with 1% BSA (bovine serum albumin), 0.1% Triton X-100 in PBS for 30 min at room temperature. Immunostaining of the microtubules was performed by treating the cells first with a primary antibody against alpha-tubulin (anti alpha-tubulin, mouse monoclonal antibody) followed by the incubation with a secondary antibody conjugated to AlexaFluor[®]-488 (goat anti-mouse IgG-AlexaFluor[®]-488, Cell Signaling Technology) for 1 h in the dark. Then, the glass coverslips were mounted in 4-88-based mounting medium containing 1 μ g/mL DAPI (4',6-diamidino-2-phenylindole) for counterstaining the nuclei and 2.5% DABCO (1,4-diazabicyclo[2.2.2]octane). Alterations of the microtubule cytoskeleton were documented by fluorescence microscopy using a Zeiss Imager A1 AX10 (400 \times magnification).

2.3.9. Cell cycle analyses

HT-29 colon carcinoma, MCF-7 breast cancer and 518A2 melanoma cells (5×10^4 cells/mL, 3 mL/well) grown in 6-well plates were allowed to adhere for 24 h. First, various concentrations of the

test compounds or vehicle (DMF) were applied to the different cells lines for 24 h, each in a single experiment in order to estimate the range of concentrations where an effect on the cell cycle can be observed. Cell cycle analyses of concentrations within this range were then determined in three independent experiments. The cells were harvested by trypsinization and fixed in ice-cold 70% ethanol overnight. After RNA digestion and propidium iodide (PI) staining with PI staining solution (50 $\mu\text{g}/\text{mL}$ propidium iodide, 0.1% sodium citrate, 50 $\mu\text{g}/\text{mL}$ RNase A in PBS) for 30 min at 37 °C, the fluorescence intensity of 10,000 single cells was recorded with a Beckmann Coulter Cytomics FC500 flow cytometer at $\lambda_{\text{em}} = 630$ nm and $\lambda_{\text{ex}} = 488$ nm. The cell distribution of single cells (%) in G1, S and G2/M phase of the cell cycle progression as well as the proportion of sub-G1 events (apoptotic cells) were analyzed by using the CXP Analysis Software (Beckmann Coulter).

2.3.10. Zebrafish angiogenesis assay [31]

Transgenic zebrafish of the strain *Tg(fli1a:EGFP)* with a *casper* background were raised under standard conditions at 27-28 °C [32,33]. After manual dechoriation at 24-26 hpf the embryos were transferred into 6-well plates [5 embryos/well in 5 mL E3 medium (5 mM NaCl, 0.17 mM KCl, 0.33 mM CaCl₂, 0.33 mM MgSO₄, 0.01% methylene blue, pH 7.2)] and treated with **3b-c** (0.5 and 1 μM), or vehicle (DMF) for 48 h. The development of the SIV (subintestinal veins) was documented by fluorescence microscopy ($\lambda_{\text{ex}} = 488$ nm, $\lambda_{\text{em}} = 509$ nm, Leica MZ10F with ZEISS AxioCam Mrc and Mrc-ZEN pro 2012 software). The SIV length of at least 17 identically treated fish was quantified as mean \pm SD with vehicle treated controls set to 100%. Significant deviations from the control data were determined using a t-test. *: $p < 0.001$.

3. Results and discussion

3.1. Chemistry

The naphthopyrans **2a-b** were synthesized by a base-catalyzed one-pot reaction of malononitrile with 3-pyridinaldehyde/4-pyridinaldehyde and 1-naphthol as previously described (Scheme 1) [25]. **2c-d** were prepared analogously by reaction of malononitrile with 3-pyridinaldehyde/4-pyridinaldehyde and 4-chloro-1-naphthol. The compounds precipitated from the reaction solution after a short time and were obtained as pure solids in moderate to high yields. The reaction of **2a-d** with $[\text{Ru}(p\text{-cymene})\text{Cl}_2]_2$

afforded the corresponding Ru(II) complexes **3a-d** as brown solids in yields ranging from 71% to 84%.

As is known for other ruthenium(II)-arene complexes [2], complexes **3a-d** underwent activating hydrolysis to give aqua complexes in ^1H NMR experiments in aqueous solvent mixtures. Their formation increased with the amount of water present and with time of exposure, reaching a maximum after 48 h. It could be attenuated by addition of NaCl. In contrast, the conversion of the starting dichlorido complexes was expedited by the addition of AgNO_3 . (*cf.* Supplementary data, Figures S1–S5).

((Scheme 1 near here))

3.2. Antiproliferative activity

The antiproliferative activity of the compounds was investigated by MTT assays [34]. They were tested against a panel of eight cancer cell lines of six different entities, as well as against the non-malignant human dermal fibroblasts HDFa (Table 1). Apart from naphthopyrans **2a-b**, all test compounds showed dose dependent inhibitory curves against the whole panel of cancer cell lines in the range of double-digit nanomolar to single-digit micromolar IC_{50} values. In our standard concentration range no vital cells were detected for **2a-b** after 72 h. Due to this enormous toxicity, we desisted from further investigations of these two compounds. In contrast, RuPy, the known complex $\text{Ru}(\eta^6\text{-}p\text{-cymene})\text{Cl}_2(\text{pyridine})$, bearing pyridine instead of the naphthopyran ligands, had no influence on the cell viability even at concentrations as high as 100 μM . Hence, the cytotoxicity of the pertinent (arene)ruthenium(II) complexes **3a-b** with IC_{50} values ranging from double-digit nanomolar to single-digit micromolar can presumably be attributed to the naphthopyran ligands **2a** and **2b**, the toxicity of which is obviously attenuated by their complexation to the ruthenium fragment. The analogous reduction of cytotoxicity by ruthenation was less pronounced and not observed for all cell lines in the case of the chloro-naphthopyrans **2c-d** and their complexes **3c-d**. It is also noteworthy that the complexes **3a-d** are distinctly more cytotoxic than cisplatin. Moreover, tentative structure-activity relationships and selectivities emerged for the complexes **3a-d**. On average, the 3-pyridinyl derivatives **3a** and **3c** were slightly more active than their respective 4-pyridinyl congeners **3b** and **3d**, while the unchlorinated derivatives **3a** and **3b** were more cytotoxic than their respective chloro congeners **3c** and

3d. When we measured the uptake rates of the complexes **3a-d** by determining the ruthenium content in HT-29 and HCT-116 colon carcinoma cells after 3 h exposure, there was no significant difference between the less cytotoxic complexes **3c-d** and the more cytotoxic complexes **3a-b** (*cf.* Supplementary data). Hence, the difference in cytotoxicities between **3a-b** and **3c-d** must originate from different target interactions or general modes of action rather than from differences in the uptake rates. In addition, complexes **3a-d** showed a distinct selectivity for certain cell lines. On average, the multi-drug resistant (MDR) cancer cell line MCF-7^{Topo}, which overexpresses the ABC (ATP-binding cassette)-transporters BCRP (breast cancer resistance protein), as well as the pancreatic adenocarcinoma cells Panc-1 were most sensitive to complexes **3a-d**, while the colon carcinoma cells HT-29 and HCT-116 were least sensitive. Since the IC₅₀ values of the complexes **3a-d** in the MDR cell lines KB-V1^{Vbl} and MCF-7^{Topo}, overexpressing P-gp (P-glyco protein) and BCRP, respectively, were equal to or even lower than those in the other cell lines, it can be assumed that the complexes **3a-d** are not substrates of P-gp and BCRP. Interestingly, complexes **3a-d** showed also a distinct selectivity for tumor cells over non-malignant dermal fibroblasts (HDFa), which were hardly affected even at concentrations of 100 μM.

((Table 1 near here))

3.3. DNA interaction

Since (arene)ruthenium(II) complexes are known to bind to DNA, we investigated the interaction of complexes **3a-d** with DNA in several cell-free assays [10,35]. Their influence on the electrophoretic mobility of the different topological forms of pBR322 plasmid DNA was monitored by EMSA (Figure 2). To exclude that the naphthopyran ligands themselves cause any band shifts, the plasmid DNA was incubated with the ruthenium complexes **3a-d** as well as with the naphthopyrans **2a-d**. The complexes caused a slight shift whereas no interaction was observed for the ligands. The finding that the chloro-substituted complexes **3c** and **3d** led to a more distinctly decreased mobility when compared with **3a** and **3b** does not correlate with the cytotoxicities of the complexes. In addition, the shifts induced by the ruthenium complexes differed noticeably from that caused by cisplatin. The test compounds gave rise to only a slight shift of the band of the fast-moving supercoiled *ccc*-topoform whereas the mobility of the slowly moving open circular *oc*-topoform was not influenced. In contrast, cisplatin gave rise to

pronounced mobility changes of both forms. At a dose of 25 μM of cisplatin only one band was observed whereas higher concentrations even induced the rewinding of the plasmid DNA which increased the electrophoretic mobility of the DNA again.

((Figure 2 near here))

The interaction of compounds **3a-d** with DNA was confirmed in a fluorescence-based staining assay (Figure 3 A). Salmon sperm DNA (ssDNA) was first incubated with the test compounds at various concentrations and then stained with ethidium bromide (EtBr). Then, the fluorescence intensity of the EtBr-DNA adducts was measured. It is typically reduced if the test compounds inhibit the intercalation of EtBr into DNA by morphological distortions of the latter as a consequence of binding interactions. As in the EMSA, no DNA interaction was detected for the naphthopyran ligands **2a-d** in these EtBr-assays (*cf.* Supplementary data), while complexes **3a-d** reduced the EtBr fluorescence significantly to values $< 20\%$ compared to vehicle treated controls. By using FAAS and absorption spectroscopy, we determined the degree of ruthenation of calf thymus DNA over time. The amount of ruthenium associated with DNA increased with time (Figure 3 B). The times at which the metal load of the DNA reached 50% were 19, 16, 9 and 8 min for **3a**, **3b**, **3c** and **3d**, respectively. These results indicate that the rates of binding of **3a-d** to natural double-helical DNA are markedly higher than those of cisplatin ($t_{50\%} \sim 120$ min) [36]. The marginal shift of pBR322 plasmid DNA in EMSA assays, on the one hand, and the much greater reduction of EtBr fluorescence in EtBr assays and the higher DNA binding rates of **3a-d** compared to cisplatin, on the other hand, suggest a DNA binding mode and bond strength for **3a-d** that are different from that of cisplatin. The ruthenium complexes **3a-d**, like RAPTA-C, are likely to form adducts with DNA mainly at the purine sites with a lower bond strength compared to cisplatin [10]. We assume that the ruthenium complexes were detached from DNA during electrophoresis which caused the smaller shift in EMSA.

((Figure 3 near here))

3.4. Effects on the cell cycle progression

Naphthopyrans such as LY290181 are known to induce the accumulation of cells in G2/M phase of the cell cycle. [19] Therefore, we investigated the influence of **3a** and **3b** on the cell cycle progression

in HT-29 colon carcinoma, 518A2 melanoma, and MCF-7^{Topo} breast cancer cells (Figure 4). In 518A2 melanoma cells, both complexes induced a dose-dependent accumulation of cells in G2/M phase and the decrease of cells in the G1 phase whereas the percentage of cells in S phase was barely changed. At higher concentrations, we found a distinct increase of apoptotic cells in sub-G1 (*cf.* Supplementary data). Similar rapidly increasing proportions of apoptotic sub-G1 events had previously been observed by our group for combretastatin A-4 derivatives in 518A2 melanoma cells. [37] This sensitivity to MDA-treatment might be attributed to the high proliferation rate of this particular cell line. Interestingly, the test compounds' influence on the cell cycle progression of MCF-7^{Topo} breast cancer cells differed from that in 518A2 cells. At low concentrations of **3a** (10 nM) and **3b** (25 nM), we observed a slight accumulation of cells in G1 phase which was mainly due to the decrease of the percentage of cells in the S phase whereas the proportion of cells in G2/M was not significantly altered. However, at higher concentrations we observed the arrest of cells in G2/M phase whereas the percentages of cells in G1 and in S phase were reduced. Similar effects were observed for other microtubule targeting agents at low concentrations.[38,39] Even though these concentrations cause alterations of the microtubule dynamics, prolonged mitosis and the increase of p53 expression, they might not suffice to keep all cells from passing through mitosis but are probably sufficient to induce a post-mitotic p53-dependent G1-arrest.[38,39] Higher concentrations cause the canonical G2/M arrest. However, this phenomenon is not observed in all cell lines equally.[38] In HT-29 colon carcinoma cells, **3a** and **3b** derivatives elicited a dose-dependent increase of cells in G2/M phase whereas those in S and G1 phases were decreased. HT-29 cells were also arrested in G2/M phase when treated with **2c-d** (100 nM) or **3c-d** (250 nM) (*cf.* Supplementary Data). However, the arrest was more pronounced for **2c** and **3a-c** than for **2d** and **3d**. The slighter increase of apoptotic sub-G1 events in MCF-7^{Topo} and HT-29 cells is presumably due to the incubation time of only 24 h being too short for them entering into apoptosis as consequence of the mitotic arrest in contrast to the rapidly proliferating 518A2 cells for which this short space of time seems to be sufficient.[37,40,41]

((Figure 4 near here))

The increase of cells in G2/M can be attributed to the interference of naphthopyrans with the tubulin dynamics which prevents the normal microtubule formation [19,42]. Thus, cells are kept from dividing

and arrested in mitosis for want of a functional spindle apparatus. Since the standard cell cycle analyses cannot distinguish between G2 and mitotic cells we additionally stained the nuclei of HT-29 cells treated with **3a-d** and counted the percentage of mitotic cells with condensed DNA. After exposing the cells to the test compounds in the highest applied concentrations of the cell cycle analyses (100 or 250 nM; 6h), the proportion of mitotic cells was found to be significantly increased (*cf.* Supplementary data). While only 7% of control cells were mitotic, the mitotic indices of cells treated with **3a** (250 nM) and **3b** (250 nM) were increased markedly to 27% and 24%, respectively. The incubation with 250 nM of the chlorinated derivatives **3c** and **3d** caused a lesser accumulation of mitotic cells (20% and 15%, respectively).

3.5. Effects on the cytoskeletal organization

Since blocking of cell division and mitotic arrest are typical consequences of the treatment with tubulin-binding agents, we additionally investigated the effects of complexes **3a-d** on microtubule organization in 518A2 melanoma cells (Figure 5) [16]. In order to visualize early effects on the microtubule cytoskeleton, we first exposed the cells to the test compounds **3a-d** for 3 h. Slight alterations in the tubulin dynamics caused by low concentrations of MDA might affect apoptosis induction, migration or angiogenesis, which are, however, hard to recognize with the naked eye. Therefore, we chose higher concentrations of the test compounds (500 nM) just to visualize the potential microtubule destabilizing effect of the complexes. While **3a** caused a complete disruption of the microtubules, **3b-c** eroded the microtubule cytoskeleton but left some clusters of intact microtubules. Complex **3d**, the test compound with the highest IC₅₀ value against these cells, induced no distinct alteration of the microtubule organization. We additionally tested the microtubule destructing effect of **3a** and **3b** (both 60 nM, 24 h) in 518A2 cells and also found alterations of the microtubule cytoskeleton (*cf.* Supplementary data). Even though some filamentous microtubules were observed in cells treated with **3a** and **3b**, there were areas with destroyed microtubules where tubulin was just diffusely spread. However, there were also fragmented nuclei typical of apoptosis induction. Therefore, the inhibition of tubulin polymerization was confirmed for **3a** and **3b** *in vitro* by using a turbidimetric-based cell-free assay with purified pig brain tubulin (*cf.* Supplementary data).

((Figure 5 near here))

3.6. Effect on the vasculature

Targeting tumor vasculature is still a promising approach to inhibit tumor growth [43]. While anti-angiogenic agents prevent the formation of new blood vessels, vascular-disrupting agents attack the blood supply by destruction of already established tumor blood vessels. Since the disruption of the microtubular cytoskeleton as caused by complexes **3a-d** results in the mechanical destabilization of treated cells and in alterations of cell to cell junctions which might induce the shut-down of the abnormal and fragile tumor vasculature, we surmised that complexes **3a-d** might also be vascular-disruptive [16].

The vascular-disruptive effect of complexes **3a-d** was tested on the chorioallantoic membrane (CAM) of fertilized chicken eggs. The compounds were applied topically onto the CAM in a small ring of silicon foil next to some main blood vessels. Any alterations of the blood vessels were documented 0, 6 and 24 h post application (hpa). However, these tests were hampered by the poor solubility profile of some test compounds. Only complexes **3b** and **3c** did not precipitate under the conditions of the CAM assay. They induced the disruption of even big blood vessels and consequently caused hemorrhages at 6 hpa (Figure 6 B). 24 hpa an extensive destruction of the vasculature was observed.

Besides the conventional blood vessel formation via angiogenesis, which is mediated by proliferating and migrating endothelial cells, alternate mechanisms such as vascular mimicry by cancer cells play a vital role in the maintenance of the tumor vessel network, which supports tumor growth, metastasis and invasion [44-46]. Hence, the effect of the test compounds on neovascularization via vascular mimicry was studied by tube formation assays using U-87 glioblastoma cells [47]. These cells form tubular blood vessel-like networks when grown on thin layers of matrigel (Figure 6 A). In contrast to the complex tubular and cord-like networks formed by untreated control cells, cells treated with complexes **3b** or **3c** were diffusely spread throughout the well showing no signs of blood vessel-like formations. As to MTT assays, the vitality of the treated cells was greater than 80% compared to untreated U-87 cells so that antiproliferative effects of the compounds can be excluded.

((Figure 6 near here))

The microtubule destruction caused by compounds **3a-d** might also contribute to their anti-angiogenic effect via alterations of cell-cell contacts, reduced cell migration and inhibition of sprout formation [16]. In addition, it is known that (arene)ruthenium(II) complexes show anti-angiogenic activity originating from their binding to proteins or enzymes and subsequent inhibition of angiogenesis-relevant growth factor receptors such as fibroblast growth factor receptor (FGF-R1) or vascular endothelial growth factor receptor (VEGFR) [13]. Therefore, we investigated whether the new compounds affect the establishment of new blood vessels *in vivo* in *Tg(fli1a:EGFP)* zebrafish embryos with *casper* background [32,33]. Due to their transparency, the effect of test compounds on the formation of SIV, blood vessels that absorb nutrients from the yolk and develop between 48-72 hpf, could simply be monitored by fluorescence microscopy [48,49]. While vehicle-treated zebrafish embryos developed the typically sinoidal structure with a ladder rung-like pattern, the SIV of embryos treated with non-toxic concentrations of complexes **3b-c** were significantly underdeveloped (Figure 7). The SIV of fish treated with **3b** were much smaller and the ladder rungs incomplete and deficient whereas in fish exposed to **3c** the SIV were only rudimentary and barely visible. The area covered by SIV was quantified using the ImageJ software and the one of untreated control fish set to 100%. The SIV area in zebrafish embryos treated with **3b** (1 μ M) was developed to 43% compared with the control fish whereas the SIV area of **3c** (1 μ M) treated fish was developed to only 10% compared to control.

((Figure 7 near here))

4. Conclusions

The (arene)ruthenium(II) complexes **3a-d** of 4-aryl-4*H*-naphthopyrans represent a new class of selective and potent anti-cancer agents addressing multiple targets by combining the individual effects of the naphthopyrans and the (arene)Ru(II) fragment in a beneficial manner. They retained the DNA-binding ability, typical of (arene)ruthenium(II) complexes, augmented by the anti-angiogenic, vascular-disruptive and cytotoxic activities of the naphthopyrans. By coordination to the (*p*-cymene)Ru(II) fragment even the brutal toxicity of the unchlorinated naphthopyrans **2a** and **2b** was attenuated and the resulting complexes **3a** and **3b** showed manageable cytotoxicities and a distinct selectivity for cancer over non-malignant cells. However, they were still distinctly more cytotoxic on

average than their chlorinated congeners **3c** and **3d**. The preliminary DNA binding studies revealed that the new complexes **3a-d** bind about 10 times faster and in a different way to calf thymus DNA when compared to cisplatin. We assume that the complexes **3a-d**, like RAPTA-C, preferentially bind to the purine sites of DNA [10]. It cannot be excluded that these lesions might induce DNA repair mechanisms, which eventually elicit apoptosis. However, the apoptosis induction is more likely the result of the alterations of the microtubule cytoskeleton, which is another major target of the new complexes, apparent from its extensive destruction and a subsequent mitotic arrest of treated cells. As a corollary of this effect, we observed a weakening of the cell-to-cell junctions of endothelial cells resulting in the disruption of the vasculature in the chorioallantoic membrane of chicken eggs or in an impairment of the angiogenesis in zebrafish. The new pleiotropic ruthenium complexes **3a-d** are to be tested now in *in vivo* xenograft studies.

Abbreviations

ABC, ATP binding cassette; BCRP, breast cancer resistance protein; CAM, chorioallantoic membrane; ccc, covalently closed circular; DAPI, 4',6-diamidino-2-phenylindole; dpf, days past fertilization; EMSA, electrophoretic mobility shift assay; EtBr, ethidium bromide; FGF-R1, fibroblast growth factor receptor 1; hpa, hours past application; hpf; hours past fertilization; MDA, microtubule destabilizing agent; MDR, multi-drug resistant; MTT, 3-(4,5-dimethylthiazol-2-yl)-2,5-diphenyltetrazolium bromide; oc, open circular; P-gp, P-glycoprotein; PI, propidium iodide; SD, standard deviation; SIV, subintestinal veins; ssDNA, salmon sperm DNA; VDA, vascular-disrupting agent; VEGFR, vascular endothelial growth factor receptor

Acknowledgement

RS thanks the Deutsche Forschungsgemeinschaft for a grant (Scho 402/12), JK and VB thank the Czech Science Foundation for a grant (17-05302S).

Supplementary data. Methods used for cellular uptake studies, determination of the mitotic index, fluorescence labeling of microtubules, tubulin polymerization assay; additional results from stability studies, cellular uptake studies, EtBr-assays, cell cycle analyses, mitotic index determinations, and effects on microtubules at doi: xxxx

References

- [1] B. Rosenberg, L. Van Camp, T. Krigas, *Nature* 205 (1965) 698-699.
- [2] C.M. Clavel, E. Paunescu, P. Nowak-Sliwinska, A.W. Griffioen, R. Scopelliti, P.J. Dyson, *J. Med. Chem.* 58 (2015) 3356-3365.
- [3] S. Page, R. Wheeler, *Educ. Chem.* (2012) 26-29.
- [4] S. Leijen, S.A. Burgers, P. Baas, D. Pluim, M. Tibben, E. van Werkhoven, E. Alessio, G. Sava, J.H. Beijnen, J.H.M. Schellens, *Invest. New Drugs* 33 (2015) 201-214.
- [5] C.G. Hartinger, M.A. Jakupec, S. Zorbas-Seifried, M. Groessler, A. Egger, W. Berger, H. Zorbas, P.J. Dyson, B.K. Keppler, *Chem. Biodivers.* 5 (2008) 2140-2155.
- [6] C.S. Allardyce, P.J. Dyson, *Platin. Met. Rev.* 45 (2001) 62-69.
- [7] A. Bergamo, L. Messori, F. Piccioli, M. Cocchietto, G. Sava, *Invest. New Drugs* 21 (2003) 401-411.
- [8] C.G. Hartinger, S. Zorbas-Seifried, M.A. Jakupec, B. Kynast, H. Zorbas, B.K. Keppler, *J. Inorg. Biochem.* 100 (2006) 891-904.
- [9] B. Biersack, *Mini Rev. Med. Chem.* 16 (2016) 804-814.
- [10] Z. Adhireksan, G.E. Davey, P. Campomanes, M. Groessler, C.M. Clavel, H. Yu, A.A. Nazarov, C.H.F. Yeo, W.H. Ang, P. Dröge, U. Rothlisberger, P.J. Dyson, C.A. Davey, *Nat. Commun.* 5 (2014) 5:3462. doi:10.1038/ncomms4462.
- [11] A. Dorcier, C.G. Hartinger, R. Scopelliti, R.H. Fish, B.K. Keppler, P.J. Dyson, *J. Inorg. Biochem.* 102 (2008) 1066-1076.
- [12] R.H. Berndsen, A. Weiss, U.K. Abdul, T.J. Wong, P. Meraldi, A.W. Griffioen, P.J. Dyson, P. Nowak-Sliwinska, *Nat. Sci. Rep.* 7 (2017) 7:43005. doi:10.1038/srep43005.
- [13] P. Nowak-Sliwinska, J.R. van Beijnum, A. Casini, A.A. Nazarov, G. Wagnières, H. van den Bergh, P.J. Dyson, A.W. Griffioen, *J. Med. Chem.* 54 (2011) 3895-3902.
- [14] W.M. Motswainyana, P.A. Ajibade, *Adv. Chem.* 2015 (2015) 859730. doi:10.1155/2015/859730.

- [15] a) R. Schobert, S. Seibt, K. Mahal, A. Ahmad, B. Biersack, K. Effenberger-Neidnicht, S. Padhye, F.H. Sarkar, T. Mueller, *J. Med. Chem.* 54 (2011) 6177-6182;
- b) B. Biersack, M. Zoldakova, K. Effenberger, R. Schobert, *Eur. J. Med. Chem.* 45 (2010) 1972-1975.
- [16] D. Bates, A. Eastman, *Br. J. Clin. Pharmacol.* 83 (2017) 225-268.
- [17] S. Kasibhatla, H. Gourdeau, K. Meerovitch, J. Drewe, S. Reddy, L. Qui, H. Zhang, F. Bergeron, D. Bouffard, Q. Yang, J. Herich, S. Lamothe, S.X. Cai, B. Tseng, *Mol. Cancer Ther.* 3 (2004) 1365-1374.
- [18] S.A. Patil, J. Wang, X.S. Li, J. Chen, T.S. Jones, A. Hosni-Ahmed, R. Patil, W.L. Seibel, W. Li, D.D. Miller, *Bioorg. Med. Chem. Lett.* 22 (2012) 4458-4461.
- [19] D.L. Wood, D. Panda, T.R. Wiernicki, L. Wilson, M.A. Jordan, J.P. Singh, *Mol. Pharmacol.* 52 (1997) 437-444.
- [20] T.R. Wiernicki, J.S. Bean, C. Dell, A. Williams, D. Wood, R.F. Kauffman, J.P. Singh, *J. Pharmacol. Exp. Ther.* 278 (1996) 1452-1459.
- [21] W. Kemnitzer, J. Drewe, S. Jiang, H. Zhang, J. Zhao, C. Crogan-Grundy, L. Xu, S. Lamothe, H. Gourdeau, R. Denis, B. Tseng, S. Kasibhatla, S.X. Cai, *J. Med. Chem.* 50 (2007) 2858-2864.
- [22] F. Schmitt, M. Gold, I. Andronache, B. Biersack, R. Schobert, T. Mueller, *Eur. J. Med. Chem.* *to be submitted*.
- [23] S.K. Singh, S. Joshi, A.R. Singh, J.K. Saxena, D.S. Pandey, *Inorg. Chem.* 46 (2007) 10869-10876.
- [24] R.E. Morris, R.E. Aird, P. del Socorro Murdoch, H. Chen, J. Cummings, N.D. Hughes, S. Parsons, A. Parkin, G. Boyd, D.I. Jodrell, P.J. Sadler, *J. Med. Chem.* 44 (2001) 3616-3621.
- [25] R. Ballini, F. Bigi, M.L. Conforti, D. De Santis, R. Maggi, G. Oppici, G. Sartori, *Catal. Today* 60 (2000) 305-309.
- [26] M. Moore, S.A. Ertem, Treatment of Ovarian Cancer with 2-amino-4H-naphtho[1,2-b]pyran-3-carbonitriles. WO/2013/070998

- [27] C.A. Vock, C. Scolaro, A.D. Phillips, R. Scopelliti, G. Sava, P.J. Dyson, *J. Med. Chem* 49 (2006) 5552-5561.
- [28] J.K. Muenzner, T. Rehm, B. Biersack, A. Casini, I.A.M. de Graaf, P. Worawutputtpong, A. Noor, R. Kempe, V. Brabec, J. Kasparikova, R. Schobert, *J. Med. Chem.* 58 (2015) 6283-6292.
- [29] C. Spoerlein-Guettler, K. Mahal, R. Schobert, B. Biersack, *J. Inorg. Biochem.* 138 (2014) 64-72.
- [30] B. Nitzsche, C. Gloesenkamp, M. Schrader, M. Ocker, R. Preissner, M. Lein, A. Zakrzewicz, B. Hoffmann, M. Höpfner, *Br. J. Cancer* 103 (2010) 18-28.
- [31] H. Draut, T. Rehm, G. Begemann, R. Schobert, *Chem. Biodivers.* 14 (2017) e1600302. doi:10.1002/cbdv.201600302.
- [32] N.D. Lawson, B.M. Weinstein, *Dev. Biol.* 248 (2002) 307-318.
- [33] R.M. White, A. Sessa, C. Burke, T. Bowman, J. LeBlanc, C. Ceol, C. Bourque, M. Dovey, W. Goessling, C.E. Burns, L.I. Zon, *Cell Stem Cell* 2 (2008) 183-189.
- [34] T. Mosmann, *J. Immunol. Methods* 65 (1983) 55-63.
- [35] G. Süß-Fink, *Dalton Trans.* 39 (2010) 1673-1688.
- [36] D.P. Bancroft, C.A. Lepre, S.J. Lippard, *J. Am. Chem. Soc.* 112 (1990) 6860-6871.
- [37] K. Mahal, B. Biersack, H. Caysa, R. Schobert, T. Mueller, *Invest. New Drugs* 33 (2015) 541-554.
- [38] B. Pourroy, M. Carré, S. Honoré, V. Bourgarel-Rey, A. Kruczynski, C. Briand, D. Braguer, *Mol. Pharmacol.* 66(3) (2004) 580-591.
- [39] Z.N. Demidenko, S. Kalurupalle, C. Hanko, C.U. Lim, E. Broude, M.V. Blagosklonny, *Oncogene* 27 (2008) 4402-4410.
- [40] C. Kanthou, G.M. Tozer, *Blood* 99 (2002) 2060-2069.
- [41] J.D. Orth, A. Loewer, G. Lahav, T.J. Mitchison, *Mol. Biol. Cell.* 23 (2012) 567-576.
- [42] D. Panda, J.P. Singh, L. Wilson, *J. Biol. Chem.* 272(12) (1997) 7681-7687.
- [43] D. Neri, R. Bicknell, *Nat. Rev. Cancer* 5 (2005) 436-446.

- [44] S. El Hallani, B. Boisselier, F. Peglion, A. Rousseau, C. Colin, A. Idbaih, Y. Marie, K. Mokhtari, J.L. Thomas, A. Eichmann, J.Y. Delattre, A.J. Maniotis, M. Sanson, *Brain* 133 (2010) 973-982.
- [45] C. Scavelli, B. Nico, T. Cirulli, R. Ria, G. Di Pietro, D. Mangieri, A. Bacigalupo, G. Mangialardi, A.M.L. Coluccia, T. Caravita, S. Molica, D. Ribatti, F. Dammacco, A. Vacca, *OncoGene* 27 (2008) 663-674.
- [46] M.J.C. Hendrix, E.A. Seftor, A.R. Hess, R.E.B. Seftor, *Nat. Rev. Cancer* 3 (2003) 411-421.
- [47] R.A. Francescone III, M. Faibish, R.A. Shao, *J. Vis. Exp.* 55 (2011) e3040. doi:10.3791/3040.
- [48] G.N. Serbedzija, E. Flynn, C.E. Willett, *Angiogenesis* 3 (1999) 353-359.
- [49] S. Isogai, M. Horiguchi, B.M. Weinstein, *Dev. Biol.* 230 (2001) 278-301.

((Tables))

Table 1. IC₅₀ values^[b] [nM, 72 h] derived from dose-response curves using MTT assays when applied to human cell lines.^[a]

	cisplatin	RuPy	2a	2b	2c	2d	3a	3b	3c	3d
518A2	5,300 ± 400 ^[c]	>100,000	<0.5	<0.5	37.0 ± 0.3	448 ± 13	37.8 ± 2.3	33.3 ± 2.9	121 ± 8	325 ± 2
518A2 (24 h)	4,800 ± 300	>100,000	-	-	>1,000	>1,000	>1,000	>1,000	>1,000	>1,000
HT-29	>100,000 ^[c]	>100,000	<0.5	<0.5	38.6 ± 4.0	966 ± 20	54.3 ± 3.1	82.0 ± 6.0	158 ± 1	319 ± 33
DLD-1	32,600 ± 2,400 ^[c]	>100,000	<0.5	<0.5	45.5 ± 4.0	390 ± 21	38.8 ± 3.1	41.4 ± 2.8	139 ± 11	219 ± 24
HCT-116	5,000 ± 400 ^[c]	>100,000	-	-	52.4 ± 3.6	251 ± 11	61.0 ± 7.0	62.5 ± 2.5	188 ± 7	280 ± 10
MCF-7^{Topo}	10,600 ± 700 ^[c]	>100,000	<0.5	<0.5	33.9 ± 1.5	139 ± 42	11.3 ± 0.5	37.4 ± 3.6	46.7 ± 1.7	195 ± 12
KB-V1^{Vbl}	>100,000	>100,000	-	-	33.0 ± 2.9	460 ± 31	12.5 ± 1.9	62.8 ± 5.9	36.5 ± 1.7	210 ± 13
Panc-1	4,800 ± 700 ^[c]	-	-	-	14.9 ± 1.9	371 ± 13	13.1 ± 1.1	35.7 ± 3.5	105 ± 9	191 ± 10
U-87	-	>100,000	-	-	254 ± 49	>1000	279 ± 47	396 ± 45	73 ± 13	>1,000
HDFa	>100,000	>100,000	-	-	-	-	>100,000	>100,000	>100,000	>50,000

[a] human cell lines: 518A2 melanoma, MCF-7^{Topo} breast adenocarcinoma, KB-V1^{Vbl} cervix carcinoma, Panc-1 pancreatic ductular adenocarcinoma, HT-29, HCT-116 and DLD-1 colon carcinomas, U-87 glioblastoma cells, and HDFa human dermal fibroblasts. [b] IC₅₀ values are the means ± SD of four independent experiments. [c] values determined by Muenzner *et al.* [28]

((Captions to Schemes and Figures))

Scheme 1. Reagents and conditions: (I) $\text{CH}_2(\text{CN})_2$, MeCN, Et_3N , rt, 90 min, 59-60% (II) $[\text{Ru}(p\text{-cymene})\text{Cl}_2]_2$, $\text{CH}_2\text{Cl}_2/\text{MeOH}$, rt, 30 min, 71-84%.

Figure 1. Structures of the Ru(III) complex NAMI-A, the “piano stool” (arene)ruthenium(II) complexes RAPTA-C $[\text{Ru}(\eta^6\text{-}p\text{-cymene})\text{Cl}_2(1,3,5\text{-triaz-7-phosphaadamantane})]$ and RuPy $[\text{Ru}(\eta^6\text{-}p\text{-cymene})\text{Cl}_2(\text{pyridine})]$, and the microtubule destabilizing naphthopyran LY290181.

Figure 2. Effects of cisplatin and compounds **2a-d** and **3a-d** on the electrophoretic mobility of circular pBR322 plasmid DNA as determined by electromobility shift assays (EMSA) after 24 h of incubation. Pictures are representative of two independent experiments.

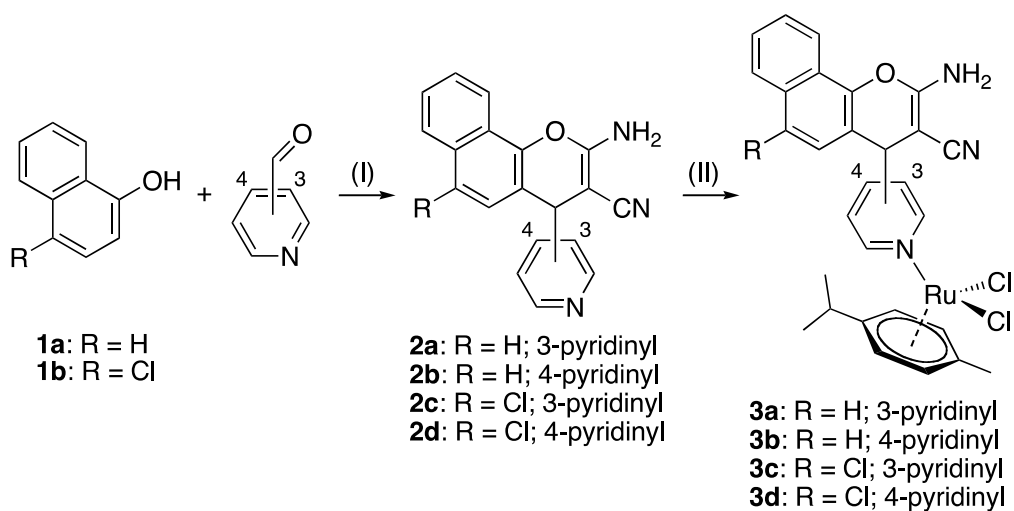
Figure 3. A) Relative ethidium bromide fluorescence after pre-incubation with vehicle (DMF; set to 100%), cisplatin, or test compounds **3a-d** (25, 50, 75, and 100 μM) for 2 h. Decreased ethidium bromide fluorescence indicates the inhibition of ethidium bromide intercalation into DNA. Significant deviations from controls (0 μM) were determined by t-test. *: p-values < 0.05. B) Kinetics of the reaction of **3a-d** with double-helical calf thymus DNA. Solutions of DNA at a concentration of 64 $\mu\text{g mL}^{-1}$ were incubated with complexes **3a-d** (8 μM) in NaClO_4 (10 mM) at 37 °C in the dark. Points represent the mean value of at least three independent experiments \pm SD.

Figure 4. Effect of **3a** and **3b** on the cell cycle progression of different cancer cell lines. Flow cytometric analyses of PI stained DNA content in 518A2 melanoma (column A), MCF-7^{Topo} breast cancer (column B), and HT-29 colon carcinoma cells (column C) after 24 h exposure to the indicated concentrations of **3a**, **3b**, and vehicle (DMF) and the distribution of cells in G1, S and G2/M phase as well as the proportion of apoptotic cells (sub-G1). The histograms are representative of at least three independent experiments.

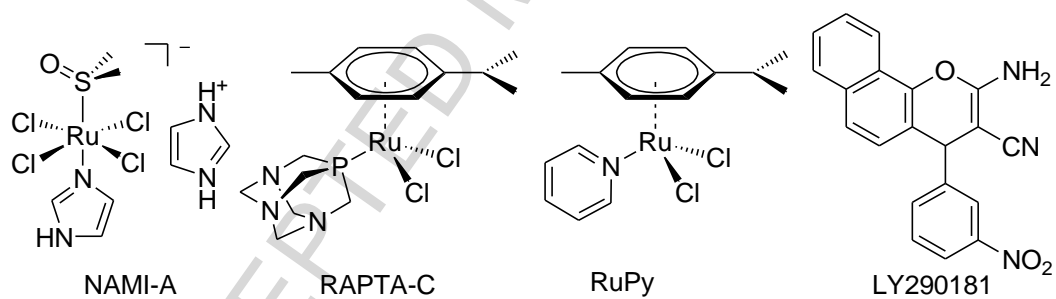
Figure 5. Effect of compounds **3a-d** (500 nM) on the organization of the microtubule cytoskeleton (green) in 518A2 melanoma cells after 3 h incubation. Nuclei were counterstained with DAPI (blue). The pictures are representative of two independent experiments (400 × magnification).

Figure 6. A) Effects of complexes **3b** (500 nM) and **3c** (1 μM) on the formation of tubular, blood-vessel-like networks by U-87 glioblastoma cells when grown on thin layers of matrigel for 24 h. Images are representative of two independent experiments (100 × magnification). Percentage of vital cells was shown by MTT assays to be > 80% compared to DMF treated control cells. B) Effects of complexes **3b** (5 nmol) and **3c** (5 nmol) when applied topically to the vasculature in the chorioallantoic membrane of fertilized chicken eggs at 6 and 24 hpa. Control: respective amount of DMF. Images are representative of at least three independent experiments (60 × magnification).

Figure 7. Effect of test compounds **3b** and **3c** on angiogenesis in zebrafish embryos. 24 hpf old transgenic *Tg(fli1a:EGFP)* zebrafish embryos were exposed to 0.5 and 1 μM of the test compounds for 48 h at 28 °C in embryo medium. A) Images are representative of at least 17 independent experiments (6.3-fold magnification). B) The area covered by subintestinal veins (SIV) was quantified using the imageJ software. The SIV area of zebrafish embryos treated with vehicle (DMF) was set to 100%. Values are the means ± SD of at least 17 independent experiments. Significant deviations from the control data were determined using a t-test. $p < 0.001$.



((Scheme 1))



((Figure 1))

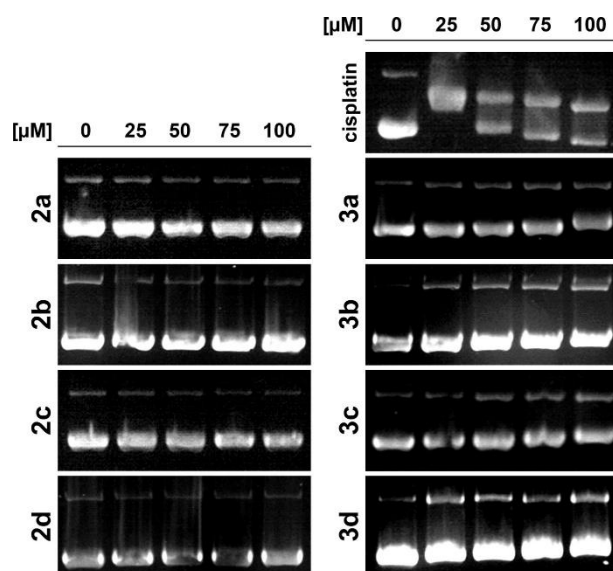


((Figure 2))

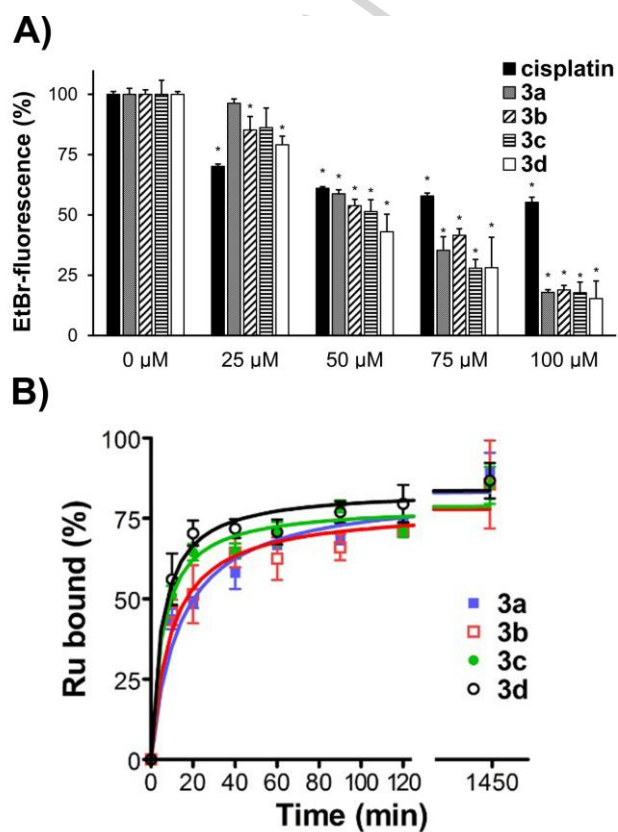


((Figure 3))

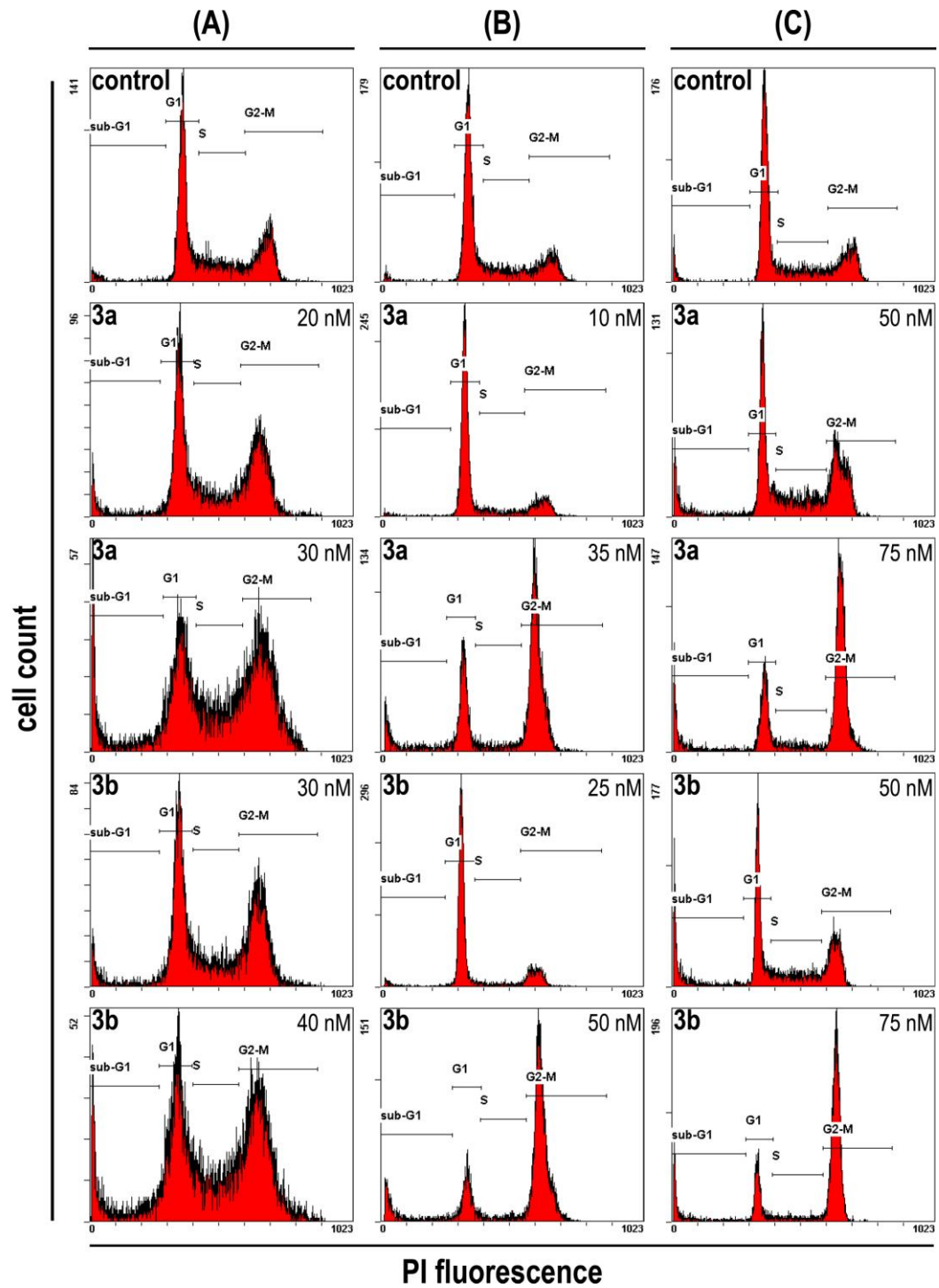


((Figure 4))

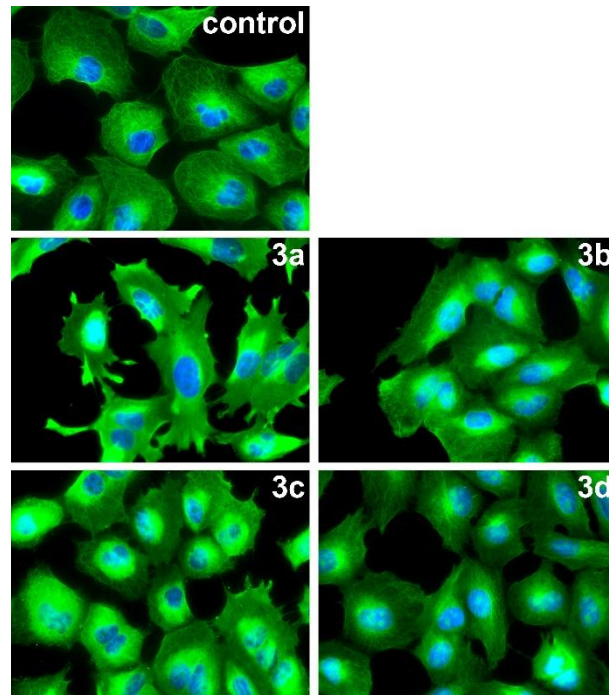


((Figure 5))

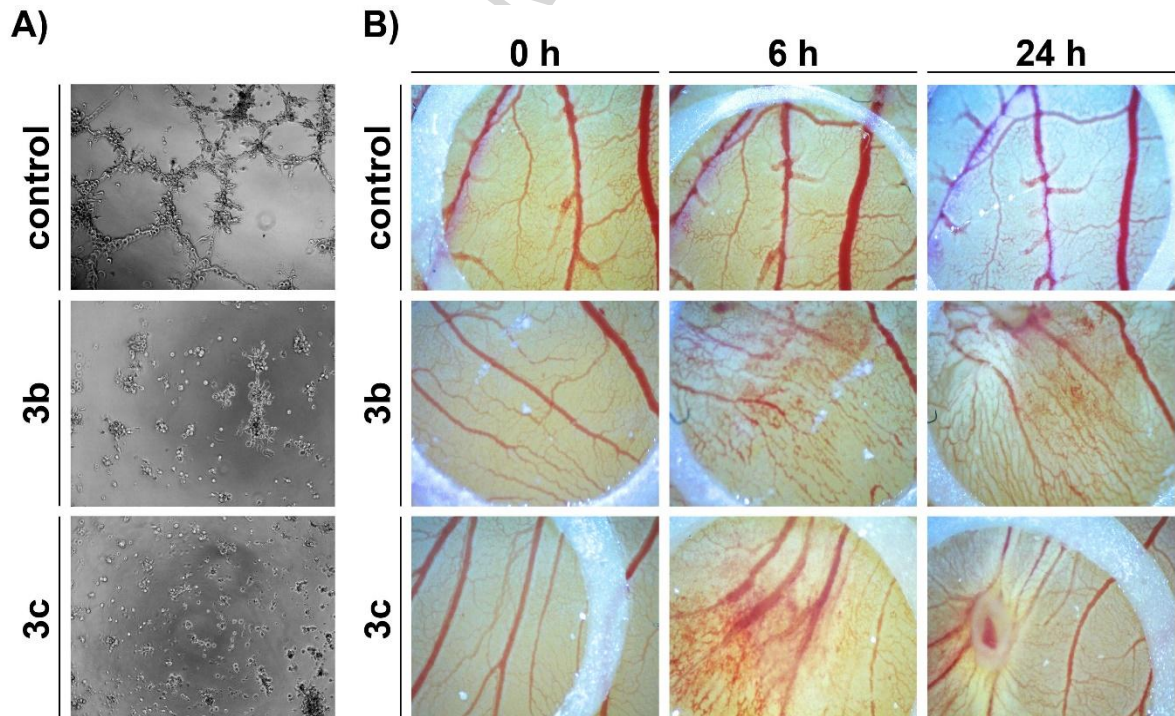


((Figure 6))

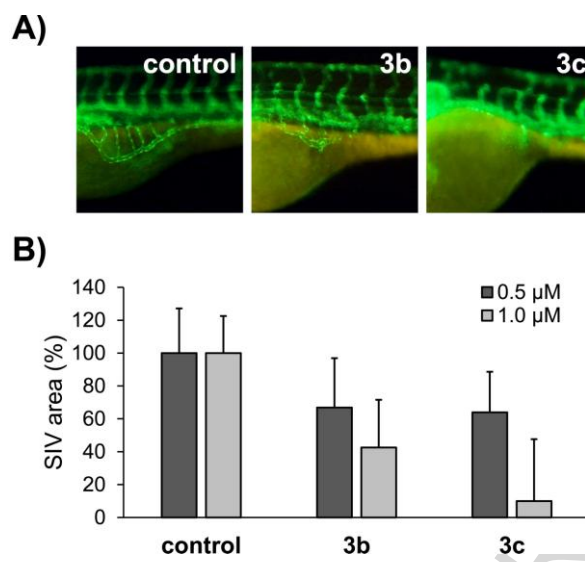


((Figure 7))

((Entry for the Table of Contents))

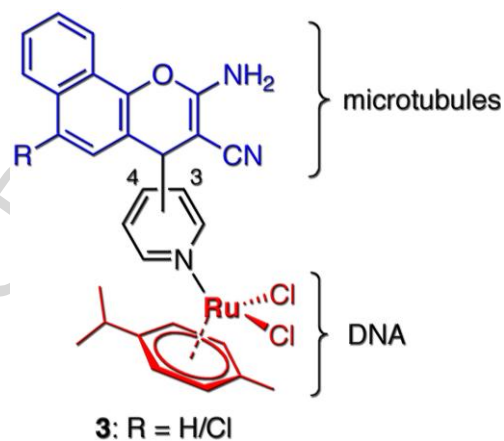
Graphical abstract

Florian Schmitt, Jana Kasparkova, Viktor Brabec, Gerrit Begemann, Rainer Schobert, Bernhard Biersack *Page – Page*

Journal of Inorganic Biochemistry xxx (2018) xxx–xxx

New (arene)ruthenium(II) complexes of 4-aryl-4*H*-naphthopyrans with anticancer and anti-vascular activities

The new complexes **3a-d** combine anti-cancer effects of naphthopyrans and a Ru(II) fragment. They bind to DNA 10 times faster and differently than cisplatin, and target the microtubular cytoskeleton causing mitotic arrest and anti-vascular effects. While active against cancer cells at nanomolar IC₅₀ concentrations they do not affect non-malignant fibroblasts.



New (arene)ruthenium(II) complexes of 4-aryl-4H-naphthopyrans with anticancer and anti-vascular activities

Highlights

- Ru(II) complexes of 4-aryl-4H-naphthopyrans **3** show selectivity for cancer cells
- **3a-d** bind to calf-thymus DNA ca. 10-times faster than cisplatin
- Complexes **3a-c** lead to alterations of the microtubule cytoskeleton
- Complexes **3b,c** are strong vascular-disrupting agents (VDA)
- **3b** and **3c** suppress angiogenesis in zebrafish embryos